Ab Initio Investigation of Intramolecular Charge Transfer States in DMABN by Calculation of Excited State X-ray Absorption Spectra

Avdhoot Datar,[*,†,¶] Saisrinivas Gudivada,[†,‡,¶] and Devin A. Matthews[*,†]

†*Department of Chemistry, Southern Methodist University, Dallas, TX 75275, USA*

‡*Present Address: Department of Physics, The University of California at Berkeley, Berkeley, CA 94720, USA*

¶*These authors contributed equally.*

E-mail: adatar@smu.edu; damatthews@smu.edu

Abstract

Dual fluorescence in 4-(dimethylamino)benzonitrile (DMABN) and its derivatives in polar solvents has been studied extensively for the past several decades. An intramolecular charge transfer (ICT) minimum on the excited state potential energy surface, in addition to the localized low-energy (LE) minimum, has been proposed as a mechanism for this dual fluorescence, with large geometric relaxation and molecular orbital reorganization a key feature of the ICT pathway. Herein, we have used both equation-of-motion coupled-cluster with single and double excitations (EOM-CCSD) and time-dependent density functional (TDDFT) methods to investigate the landscape of excited state potential energy surfaces across a number of geometric conformations proposed as ICT structures. In order to correlate these geometries and valence excited states in terms of potential experimental observables, we have calculated the nitrogen

K-edge ground and excited state absorption spectra for each of the predicted "sign-post" structures, and identified several key spectral features which could be used to interpret a future time-resolved x-ray absorption experiment.

Introduction

Since the discovery of dual fluorescence in 4-(dimethylamino)benzonitrile (DMABN, Fig. 1),[1] the valence excited electronic states of DMABN and their evolution following photoexcitation have been studied extensively to gain mechanistic understanding of this phenomenon.[2–9] Initially the state reversal model was proposed to explain the dual fluorescence.[10] In the context of this model, it was suggested that initial excitation to the lowest absorption band leads to population of S_1 and S_2 states. Internal conversion from the S_2 state followed by intramolecular vibrational relaxation (IVR) on the S_1 potential energy surface (PES) leads to "normal" fluorescence from the S_1 minimum. Alternatively, the "anomalous" fluorescence, which is sensitive to solvent polarity and temperature, was attributed to the S_2 minimum. Based on the nature of the orbitals taking part in these electronic excitations, the S_1 state is termed the locally excited (LE) state, while the S_2 state is classified as an intramolecular charge transfer (ICT) state. Grabowski et. al. suggested a mechanism that involved, on the ICT PES, twisting of the amino group relative to the aryl ring reaching an angle of 90°.[11,12] This proposed minimum on the ICT PES is denoted the twisted ICT (TICT) structure. Later, it was shown that this TICT state cannot be populated via direction absorption.[13]

Various models that have been proposed to explain the anomalous fluorescence mainly differ in the minimum energy structure assigned to the ICT state.[14] In contrast the the model outlined above, the wagging motion of the dimethylamino group was also suggested as a primary coupling mode of the LE and ICT states, which leads to a proposed wagged ICT (WICT) structure.[15,16] A model based on a planar minimum (with respect to the amino pyramidalization angle) was also put forth giving a planar ICT (PICT) state.[17–19] Additionally, a bending on the cyano group within the plane of the aryl ring, in principle produced

by a rehybridization of the cyano nitrogen orbitals from sp to sp^2, leads to a rehybridized ICT (RICT) hypothesis.[20,21] Lastly, a partially-twisted ICT geometry, as opposed to the full 90° twist angle of TICT, is suggested to be responsible for driving population of the ICT state from the wagged ground state geometry, giving a partially-twisted ICT (PTICT) state.[22] Each of these models invoke only LE and ICT states and their associated PESs as a mechanism for explaining dual fluorescence; we also mention for completeness another study where it was proposed that a third $\pi\sigma^*$ state takes part in the mechanism along with LE and ICT states.[23]

Although the TICT model is the most well-established mechanism of dual fluorescence in DMABN, vigorous ongoing debate fuels the investigation of other models as well as efforts to probe the finer details of the mechanism. Despite various theoretical approaches to understand the fluorescence mechanism, there exists no unambiguous model that can explain this phenomenon, and a cohesive description based on simple models is elusive.[7] As discussed by Köhn and Hättig, a central goal of the theoretical study on this problem is to test various models for consistency and to offer a prediction that can be investigated in experimental studies.[8]

In this work we follow the spirit of Köhn and Hättig and compute the excited state x-ray absorption spectra (ES-XAS) of multiple valence excited states at several geometries relevant to potential dual-fluorescence pathways. X-ray absorption spectroscopy (XAS), as it involves excitation of core-level electrons to the unoccupied valence/Rydberg orbitals, is an effective technique to study the local electronic as well as geometrical structure. Another attractive aspect of XAS is that it provides atomic specificity. Thus, high-resolution XAS is widely applied as a powerful technique for determining the local structure of molecular systems.[24–28] While XAS provides a useful static picture, time-resolved XAS (tr-XAS) spectroscopy is employed for tracking dynamical processes, such as solute-solvent interactions, evolution of photoexcited states, intramolecular charge transfer processes, etc. With recent advancements in experimental techniques, tr-XAS is regularly used to study condensed phase systems.[29–31]

Our calculations of the nitrogen K-edge (N1s) ES-XAS of DMABN will inform potential experimental studies by providing detailed, geometry- and state-dependent excited state XAS features and their interpretation in terms of molecular orbitals via natural transition orbitals (NTO) analysis.

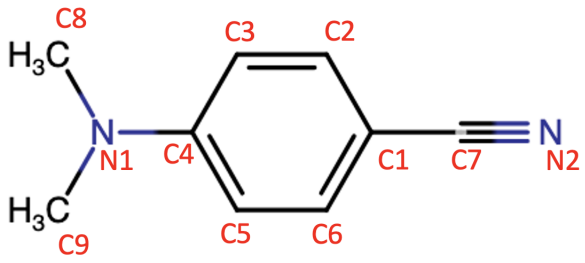

Figure 1: Schematic structure of DMABN with non-hydrogen atoms labelled with numbers.

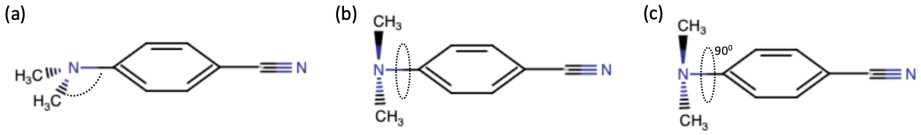

Figure 2: The structure obtained from ground and excited state optimizations (a) wagged, (b) partially-twisted, and (c) twisted.

Computational Details

The ground and excited state geometries were optimized using coupled cluster with single and double excitations (CCSD)[32–34] and equation-of-motion CCSD (EOM-CCSD)[35–37] methods, respectively. The EOM-CCSD method was also used to optimize the conical intersection (CI) geometry along the intersection seam.[38] X-ray absorption spectra were simulated using the core-valence-separated equation-of-motion coupled cluster with single and double excitations (CVS-EOM-CCSD).[39] All XAS spectra were broadened using a Gaussian profile with a standard deviation of 0.2 eV. The Pople-style basis sets provide a remarkable compromise

between the computational cost and the accuracy for XAS calculations.[40,41] Hence, the Pople split-valence triple-ζ basis set with diffuse and polarization functions, 6-311++G**,[42,43] was used for all calculations, unless specifically noted. Optimizations and (ES-)XAS calculations were performed with a development version of the CFOUR software package.[44] Natural transition orbitals (NTOs) were used to identify the nature of the excited states.

To better understand the effects of geometry on the ES-XAS, molecular geometries were also optimized using DFT methods. The ground state geometry was obtained with the M06-2X exchange-correlation functional.[45] The excited state and CI geometry optimizations were performed using the BHHLYP exchange-correlation functional[46] and the Tamm-Dancoff approximation[47,48] of time-dependent density functional theory (TDDFT). While the M06-2X functional is suitable for optimizing ground state geometries, the BHHLYP functional has been shown to perform well for optimizations of CI geometries.[49] Thus, for excited state optimizations the BHHLYP functional was chosen. These calculations were performed using the Q-Chem software package.[50] Valence and core excitation energies, oscillator strengths, and dipole moments for these geometries were then calculated using EOM-CCSD and CVS-EOM-CCSD methods as above.

Results and Discussion

Ground state structure

A slight pyramidalization of the dimethylamino group of DMABN has been established from microwave gas phase spectroscopy[51] and from x-ray diffraction in the crystalline phase[52] (as shown in Figure 2a). The wagging distortion with respect to the planar structure is observed as 15° and 11.9° in gas phase and in crystalline phase, respectively. Parusel et. al. have shown that triple-ζ quality basis sets are necessary to obtain the ground state geometry with an adequate pyramidalization angle.[53]

Our CCSD optimization of the ground state geometry leads to a non-planar structure

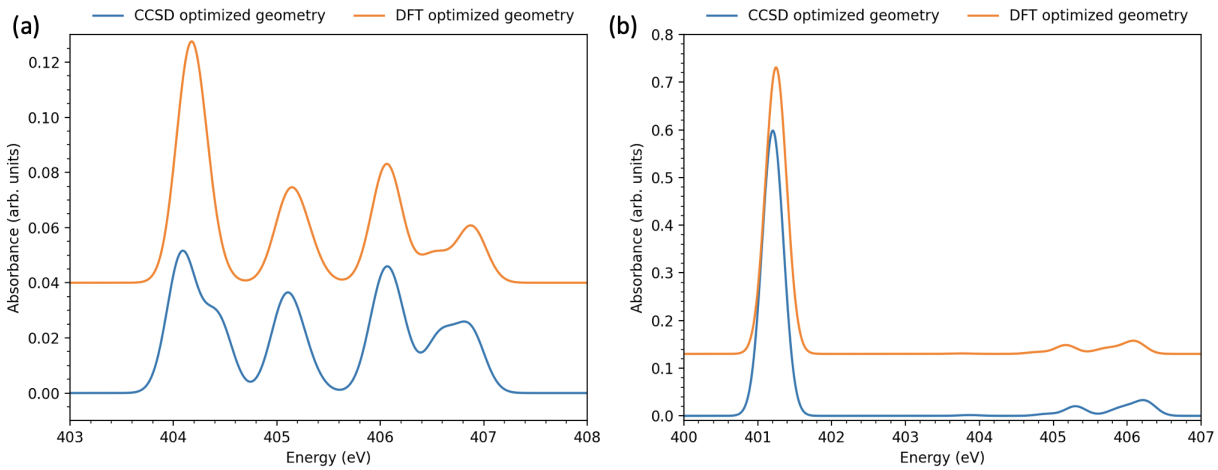

Figure 3: XAS calculation for the ground state geometries obtained from the CCSD and the DFT calculations: N1s excitation of (a) amino and (b) cyano nitrogen atoms.

with distortion along the wagging motion of the dimethylamino group (the wagging angle ω is defined as the angle between the N_1 to C_4 bond and the and plane defined by $N_1C_8C_9$; in the ground state $\omega = 30.6°$) in good agreement with the results obtained from gas phase spectroscopy.[51] Alternatively, the DFT optimization leads to a somewhat more planar structure ($\omega = 9.3°$).

Fig. 3 illustrates the effect of the pyramidalization angle on the ground state XAS. Although the spectra calculated for both the geometries is identical for N1s excitation of the cyano nitrogen, and are mostly similar for the amino nitrogen, the latter XAS spectra show a distinctive splitting of the lowest energy peak at less-planar CCSD geometry. The magnitude in the splitting is only approximately 0.4 eV, however, which is within the typical errors of relative XAS peak positions for CVS-EOM-CCSD.[54] Nonetheless with more detailed follow-up calculations this distinctive feature could then provide an additional spectroscopic measure of the ground state pyramidalization angle. The oscillator strengths of N1s excitation of the cyano nitrogen are significantly larger compared with the amino N1s excitations. The π^* orbitals of DMABN include a significant contribution from the cyano group (Table S1 of the ESI). Thus, the cyano N1s orbital has higher spatial overlap with the virtual π^* orbitals

compared to amino N1s, which is a driving factor in the higher transition dipole moments.

Valence excited states

Table 1: Excitation energies, oscillator strengths (f) and dipole moments (μ) of valence excited states at the CCSD optimized ground state geometry.

State	6-311++G**			6-311G**		
	ΔE (eV)	f	μ (D)	ΔE (eV)	f	μ (D)
LE	4.59	0.0212	8.67	4.67	0.0195	8.42
pre-ICT	4.93	0.3307	6.35	5.18	0.5751	12.07
S_3	5.24	0.2604	7.50	6.49	0.0249	2.52

It is well-established that the LE state is the lowest excited singlet state of DMABN in the Franck-Condon (FC) region, while the ICT state is the second lowest. The nature of local and charge-transfer excitations of the vertical excited states were confirmed from NTO analysis as shown in Table S2 of the ESI. Previous theoretical calculations of these states predicted a significantly higher dipole moment of the ICT state, consistent with the assignment of charge-transfer character.[5–8] However, our calculations result in a dipole moment of the ICT state lower even than that of the LE state (Table 1). The previous theoretical calculations were performed with basis sets that did not include diffuse functions, and so we recomputed the vertical excited states at the same geometry but with the non-diffuse 6-311G** basis set. The latter calculations do indeed show a significant increase in dipole moment for the ICT state, but also a drastic destabilization of the third singlet state S_3 (Table 1). Without diffuse functions, S_3 is seen to be Rydberg-like (Table S3), while the inclusion of diffuse functions leads to stabilization and mixing of S_3 with the ICT state. This mixing is then responsible for the dilution of charge-transfer character and a lowering of the dipole moment. In the non-diffuse 6-311G** basis set, the S_3 state is not truly of Rydberg character as the basis functions are not diffuse enough to capture the extended character of such states. Rather, and as seen from the NTOs (Fig. S3), the "diffuseness" of this state must co-opt valence anti-bonding orbitals which then leads to a higher energy. This comparison suggests that while

the LE state is relatively stable with respect to the quality of the basis set used, the ICT state is highly sensitive to the basis set, especially the inclusion of diffuse functions. Due to this Rydberg mixing, which is not significant at other geometries (vide infra), we denote the ICT state in the Frank-Condon region as a "pre-ICT" state. We also find a strong dependence of the ground- and excited state-XAS on diffuse functions, as illustrated in Figs. S1–S3. The DFT optimized ground state, which is nearly planar, also leads to a large dipole moment of the ICT/pre-ICT state due to a reduction in Rydberg mixing. Thus, the use of a sufficiently flexible and diffuse basis set with an accurate electronic structure method seems critical for a correct qualitative or quantitative description of the excited states of DMABN.

Table 2: Dipole moments (in Debye) of LE and ICT states for various optimized geometries calculated at the EOM-CCSD/6-311++G** level of theory. For comparison, the ground state dipole moment is 6.76 D at the EOM-CCSD/6-311++G** level.

Geometry	EOM-CCSD optimized			TDDFT optimized		
	Structure type	LE	ICT	Structure type	LE	ICT
FC	Wagged	8.67	6.35	Wagged/ planar	9.40	12.43
LE_{min}	Partially twisted	9.66	12.64	Partially twisted	9.67	9.91
ICT_{min}	Twisted	15.57	15.73	Twisted	15.10	14.71
S2/S1	Wagged with ring distortion	8.77	8.66	Wagged	9.16	5.53

Optimization of the LE state starting with the FC geometry leads directly to a minimum-energy structure denoted LE_{min}. In this structure we observe a twisting of the dimethylamino group of about 18.5°relative to the aryl ring, as depicted in Figure 2b. TDDFT optimization of LE results in a similar geometry but with a larger torsion angle of 30.5°. The torsion angle for LE_{min} obtained from EOM-CCSD optimization is in a good agreement with previous results.[8] A geometry optimization of the pre-ICT state starting at the FC geometry leads to a conical intersection seam (S_2/S_1). We further performed a minimum energy crossing point (MECP) search, which led to a wagged geometry, albeit with a smaller wag angle compared

to the ground state geometry and a distortion of the aryl ring. Similar results were obtained from the TDDFT calculations (Table 2). We found a minimum of the ICT state (ICT_{min}) at a fully-twisted geometry (Figure 2c), and were unable to find a charge-transfer minimum energy structure on the S_1 surface at any partially-twisted geometry. We were also unable to find any minimum energy structure corresponding to a rehybridized (RICT) state. The dual fluorescence of DMABN is observed in solution and is seen to depend strongly on solvent polarity, and experimentally, no dual fluorescence is observed in the gas phase.[14] While we observe the effect of the lack of polarized solvent indirectly by the absence of a low-energy pathway from the LE/ICT conical intersection to our ICT_{min} structure, the fact that a clear potential minimum with the necessary electronic and geometric features can be obtained points to the intermediate pathway as the bottleneck in non-polar solvents and the gas phase. Thus, while the kinetic facility of the ICT fluorescence pathway is highly solvent sensitive, it seems reasonable that the final ICT minimum is less sensitive.

It is notable that while both the LE_{min} and ICT_{min} structures feature a twisting of the dimethylamino group, the conical intersection which, at least according to our computed potential energy surfaces, should drive the dual fluorescence mechanism via population splitting, is found at a non-twisted geometry. Previously, Robb and co-workers have studied the topology of the extended conical intersection seam and observed that LE and ICT states are degenerate along the pyramidalization (wagging) and torsion (twisting) of dimethylamino coordinates of DMABN.[55] From that work, we can rationalize that while the minimum energy crossing point (lowest energy CI point) is at a wagged geometry, kinetically-accessible trajectories could also encounter the crossing at slightly twisted geometries. In the next section we illustrate the ramifications of the structural parameters of each of these geometries on the ES-XAS spectra.

The dipole moments of both LE and ICT states were found to increase with increasing twisting angle for the EOM-CCSD optimized structures (Table 2), although NTO analysis confirms local excitation character of S_1 at LE_{min} and charge-transfer character at ICT_{min}

(Table S5). The significant increase in dipole moment, from 6.76 D in the ground state, to almost 16 D at the ICT minimum, could also be argued to support classification of both LE and ICT states as charge-transfer states at that geometry. Investigation of the NTOs (Table S5) shows that it is not the particle NTO that is responsible for the large dipole moment, but the hole NTO, which shows a clear shift in electron density towards the dimethylamino group. We have labeled the states at ICT_{min} by correlating the character of the particle NTOs in a diabatic fashion. This observation is very similar to previous calculations performed with the RI-CC2 method.[8] On the other hand, previous calculations performed with CASSCF (on CIS optimized structures) predicted that the dipole moment of the LE state should decrease with increasing torsion angle.[5] The dipole moment of both states also increases slightly at the CI, although Rydberg mixing is still evident. Interestingly, the CI geometry is found at a larger wag angle than the ground state using TDDFT, which leads to a reduction in the ICT dipole moment.

Excited state XAS

ES-XAS spectra were calculated at the FC, LE_{min}, ICT_{min}, and S_2/S_1 geometries. The N1s core-excited states were calculated for both the amino and cyano nitrogen atoms. Transition properties such as oscillator strengths were computed with respect to the valence states S_1 and S_2 calculated as above. The spectra are labeled as "LE" or "ICT" ES-XAS, which assignment depends on the geometry—for example ICT is S_1 at ICT_{min} while it is S_2 elsewhere.

Fig. 4 shows the ES-XAS spectra for the geometries obtained from the CCSD optimizations. The amino N1s ES-XAS show strong dependence on the lower (valence) excited state and the pyramidal distortion of the dimethylamino group. A strong peak near 399 eV appears for the (pre-)ICT state (Fig. 4a, purple curve), for which a doublet-like structure emerges for LE_{min} geometry (brown curve) and splits into two peaks for CI geometry (pink curve). While for the excitation from the LE state a peak appears near 400.8 eV (Fig. 4a,

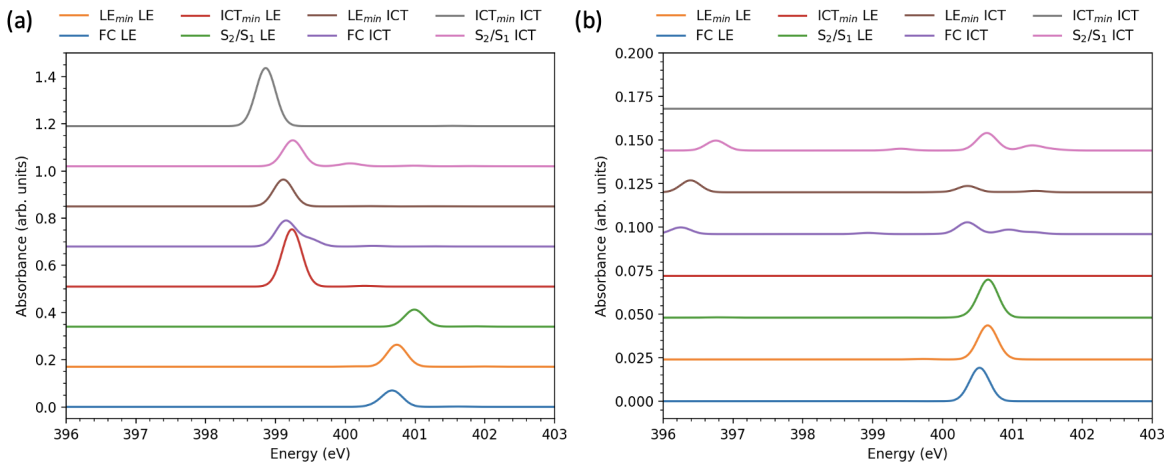

Figure 4: ES-XAS calculation for the geometries obtained from the CCSD calculations: N1s excitation of (a) amino and (b) cyano nitrogen atoms.

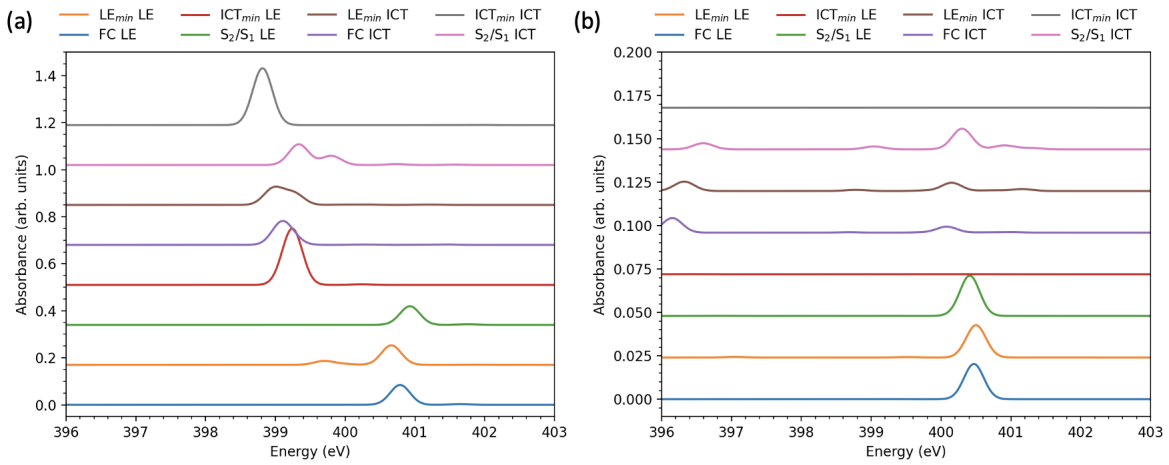

Figure 5: ES-XAS calculation for the geometries obtained from the DFT calculations: N1s excitation of (a) amino and (b) cyano nitrogen atoms.

blue curve), blue-shifting to ∼401 eV at the CI geometry (Fig. 4a, green curve). This differential signal should provide for an unambiguous identification of the relative S_1 and S_2 populations. For the fully-twisted ICT_{min} geometry, there is no ES-XAS signal at the cyano nitrogen (Fig. 4b, red and gray curves). Instead, a high-intensity peak appears in the amino nitrogen N1s spectrum for both LE and ICT states (Fig. 4a, red and gray curves). The ICT_{min} structure features a slight buildup of electron density in the cyano π^* orbital, which also results in a lengthening of the CN bond length ($\sim 0.007\mathring{A}$). These features clearly identify the ICT minimum structure in a potential tr-XAS spectrum. The cyano N1s spectra are otherwise weakly dependent on the state and geometry, with the exception of the ICT spectrum at wagged (non-twisted) geometries. There, the intensity of the peak near 400.5 eV is diminished while an additional weak peak around 396–397 eV appears. These features might also identify the transition from a wagged to twisted geometry during the dual fluorescence process. Note that the amino and cyano absorption features near 400.5 eV do overlap (the observable XAS is the sum of the amino and cyano spectra). However, the most interesting and sensitive features occur outside of this range, and with clearly different intensities. The almost complete bleaching of the x-ray absorption signal due to transitions from the cyano N1s orbital, at the ICT minimum geometry, can be attributed to the negligible overlap of this orbital with the hole NTO of all calculated transitions (see the ESI). At this geometry, the hole NTOs are uniformly polarized towards the dimethylamino group due to the change in geometry to a twisted conformation. The observable spectrum is a sum of the cyano and amino N1s absorptions, as well as convolution of the spectra originating from the various valence states and the ground state based on the relative populations. The combination of these multiple features can potentially obscure some of the finer details of the spectra, but the large differences in intensity and transition energy observed in the predicted "signpost" features suggests that they will be useful in making assignments of experimental spectra.

The ES-XAS spectra calculated at the DFT optimized structures show strikingly similar behavior (Fig. 5). Note that the nearly-planar ground state structure obtained from the

DFT optimization shows a prominent single peak near 399 eV (Fig. 5a, purple curve) for amino N1s excitation from the ICT state, in contrast to the shouldered peak in Fig. 4. Instead, the same peak at the LE_{min} and CI geometries exhibits a shoulder or complete splitting. As stated earlier, the LE_{min} geometry obtained from EOM-CCSD has a smaller twisting angle than in the TDDFT optimized structure. While the fine details of the spectra differ between the EOM-CCSD and TDDFT optimized structures, the robustness of the key spectral features is encouraging for their use in assigning potential tr-XAS spectra of the DMABN dual fluorescence mechanism.

Conclusions

We computed minimum energy structures on the ground, LE and ICT potential energy surfaces as well as the minimum energy point on the S_2/S_1 conical intersection seam using EOM-CCSD and TDDFT methods. These optimizations show overall agreement in the structural types (for example partially-twisted, twisted, wagged, etc.) for respective states, except the detailed geometrical parameters (wagging and torsional angles). The sensitivity of the pre-ICT state dipole moment at the ground state geometry to the diffuseness of the basis set hints that additional in-depth calculations of the ICT PES are required with larger basis sets and accurate electronic structure methods. The present calculations also show that some higher valence electronic states could also be important in the dual-fluorescence mechanism due to valence-Rydberg mixing.

We also computed ground and excited state x-ray absorption spectra for the lowest two valence states at various optimized structures on the ground and excited PESs. Several distinctive features are present which could be used to distinguish both the initial valence state involved in the absorption and the nature of the instantaneous nuclear geometry. We propose that the predicted spectral features could be used as spectroscopic "signposts" to assign a potential time-resolved XAS spectrum, and to distinguish between LE and ICT

fluorescence pathways in real time.

Acknowledgement

All calculations were performed on the ManeFrame II computing system at SMU. This work was supported by the Robert A. Welch foundation under grant no. N-2072-20210327 and in part by the National Science Foundation (awards OAC-2003931 and CHE-2143725).

Supporting Information Available

Electronic supplementary information files are available free of charge at the publisher's website. The following files are included:

- Supporting_Information.docx: NTOs for valence states at all discussed geometries, XAS and ES-XAS for non-diffuse basis sets.
- Supporting_Information_Raw_Data.xlsx: optimized geometries, valence-excited excitation energies and corresponding oscillator strengths, and core-excited excitation energies and corresponding oscillator strengths.

References

(1) Lippert, E.; Lüder, W.; Moll, F.; Nägele, W.; Boos, H.; Prigge, H.; Seibold-Blankenstein, I. Umwandlung von elektronenanregungsenergie. *Angewandte Chemie* **1961**, *73*, 695–706.

(2) Modesto-Costa, L.; Borges Jr, I. Discrete and continuum modeling of solvent effects in a twisted intramolecular charge transfer system: The 4-N, N-dimethylaminobenzonitrile (DMABN) molecule. *Spectrochimica Acta Part A: Molecular and Biomolecular Spectroscopy* **2018**, *201*, 73–81.

(3) Kochman, M. A.; Durbeej, B. Simulating the Nonadiabatic Relaxation Dynamics of 4-(N, N-Dimethylamino) benzonitrile (DMABN) in Polar Solution. *The Journal of Physical Chemistry A* **2020**, *124*, 2193–2206.

(4) Curchod, B. F.; Sisto, A.; Martínez, T. J. Ab initio multiple spawning photochemical dynamics of DMABN using GPUs. *The Journal of Physical Chemistry A* **2017**, *121*, 265–276.

(5) Sobolewski, A.; Sudholt, W.; Domcke, W. Ab initio investigation of reaction pathways for intramolecular charge transfer in dimethylanilino derivatives. *The Journal of Physical Chemistry A* **1998**, *102*, 2716–2722.

(6) Parusel, A. B.; Köhler, G.; Nooijen, M. A coupled-cluster analysis of the electronic excited states in aminobenzonitriles. *The Journal of Physical Chemistry A* **1999**, *103*, 4056–4064.

(7) Rappoport, D.; Furche, F. Photoinduced intramolecular charge transfer in 4-(dimethyl) aminobenzonitrile- a theoretical perspective. *Journal of the American Chemical Society* **2004**, *126*, 1277–1284.

(8) Köhn, A.; Hättig, C. On the nature of the low-lying singlet states of 4-(dimethyl-amino) benzonitrile. *Journal of the American Chemical Society* **2004**, *126*, 7399–7410.

(9) Gómez, S.; Soysal, E. N.; Worth, G. A. Micro-Solvated DMABN: Excited State Quantum Dynamics and Dual Fluorescence Spectra. *Molecules* **2021**, *26*, 7247.

(10) Lippert, E.; Lüder, W.; Boos, H. Advances in molecular spectroscopy. European Conference on Molecular Spectroscopy, Bologna, Italy, 1959r1962. 1962.

(11) Rotkiewicz, K.; Grellmann, K.; Grabowski, Z. Reinterpretation of the anomalous fluorescense of pn, n-dimethylamino-benzonitrile. *Chemical Physics Letters* **1973**, *19*, 315–318.

(12) Grabowski, Z. R.; Rotkiewicz, K.; Siemiarczuk, A.; Cowley, D. J.; Baumann, W. Twisted intramolecular charge transfer states (TICT): a new class of excited states with a full charge separation. *Nouv. J. Chim.* **1979**, *3*, 443–454.

(13) Leinhos, U.; Kühnle, W.; Zachariasse, K. A. Intramolecular charge transfer and thermal exciplex dissociation with p-aminobenzonitriles in toluene. *The Journal of Physical Chemistry* **1991**, *95*, 2013–2021.

(14) Grabowski, Z. R.; Rotkiewicz, K.; Rettig, W. Structural changes accompanying intramolecular electron transfer: focus on twisted intramolecular charge-transfer states and structures. *Chemical reviews* **2003**, *103*, 3899–4032.

(15) Zachariasse, K.; Grobys, M.; Von der Haar, T.; Hebecker, A.; Il'Ichev, Y. V.; Jiang, Y.-B.; Morawski, O.; Kühnle, W. Intramolecular charge transfer in the excited state. Kinetics and configurational changes. *Journal of Photochemistry and Photobiology A: Chemistry* **1996**, *102*, 59–70.

(16) Zachariasse, K.; Grobys, M.; Von der Haar, T.; Hebecker, A.; Il'Ichev, Y. V.; Morawski, O.; Rückert, I.; Kühnle, W. Photo-induced intramolecular charge transfer and internal conversion in molecules with a small energy gap between S1 and S2. Dynamics and structure. *Journal of Photochemistry and Photobiology A: Chemistry* **1997**, *105*, 373–383.

(17) Zachariasse, K. A. Comment on "Pseudo-Jahn–Teller and TICT-models: a photophysical comparison of meta-and para-DMABN derivatives"[Chem. Phys. Lett. 305 (1999) 8]: The PICT model for dual fluorescence of aminobenzonitriles. *Chemical Physics Letters* **2000**, *320*, 8–13.

(18) Zachariasse, K. A.; Yoshihara, T.; Druzhinin, S. I. Picosecond and nanosecond fluorescence decays of 4-(dimethylamino) phenylacetylene in comparison with those of 4-(dimethylamino) benzonitrile. No evidence for intramolecular charge transfer and a

nonfluorescing intramolecular charge-transfer state. *The Journal of Physical Chemistry A* **2002**, *106*, 6325–6333.

(19) Zachariasse, K. A.; Druzhinin, S. I.; Bosch, W.; Machinek, R. Intramolecular charge transfer with the planarized 4-aminobenzonitrile 1-tert-butyl-6-cyano-1, 2, 3, 4-tetrahydroquinoline (NTC6). *Journal of the American Chemical Society* **2004**, *126*, 1705–1715.

(20) Lewis, F. D.; Holman III, B. Singlet states of benzonitrile and p-dimethylaminobenzonitrile. *The Journal of Physical Chemistry* **1980**, *84*, 2326–2328.

(21) Sobolewski, A. L.; Domcke, W. Promotion of intramolecular charge transfer in dimethylamino derivatives: Twisting versus acceptor-group rehybridization. *Chemical physics letters* **1996**, *259*, 119–127.

(22) Coto, P. B.; Serrano-Andrés, L.; Gustavsson, T.; Fujiwara, T.; Lim, E. C. Intramolecular charge transfer and dual fluorescence of 4-(dimethylamino) benzonitrile: ultrafast branching followed by a two-fold decay mechanism. *Physical Chemistry Chemical Physics* **2011**, *13*, 15182–15188.

(23) Georgieva, I.; Aquino, A. J.; Plasser, F.; Trendafilova, N.; Köhn, A.; Lischka, H. Intramolecular charge-transfer excited-state processes in 4-(N, N-Dimethylamino) benzonitrile: The role of twisting and the $\pi\sigma^*$ state. *The Journal of Physical Chemistry A* **2015**, *119*, 6232–6243.

(24) Van Bokhoven, J. A.; Lamberti, C. *X-ray absorption and X-ray emission spectroscopy: theory and applications*; John Wiley & Sons, 2016; Vol. 1.

(25) Bunker, G. *Introduction to XAFS: a practical guide to X-ray absorption fine structure spectroscopy*; Cambridge University Press, 2010.

(26) Stöhr, J. *NEXAFS Spectroscopy*; Springer: Berlin, 1992.

(27) McNeil, B. W. J.; Thompson, N. R. X-Ray Free-Electron Lasers. *Nature Photon* **2010**, *4*, 814–821.

(28) Garg, K. B.; Norman, D.; Stern, E. A. *X-ray Absorption In Bulk And Surfaces-Proceedings Of The International Workshop*; World Scientific, 1994.

(29) Balerna, A.; Mobilio, S. Synchrotron Radiations: Basics, Methods and Applications. *Introduction to synchrotron radiation. Springer, Berlin* **2015**, *799*.

(30) Bressler, C.; Chergui, M. Molecular structural dynamics probed by ultrafast X-ray absorption spectroscopy. *Annual review of physical chemistry* **2010**, *61*, 263–282.

(31) Costantini, R.; Faber, R.; Cossaro, A.; Floreano, L.; Verdini, A.; Hättig, C.; Morgante, A.; Coriani, S.; Dell'Angela, M. Picosecond timescale tracking of pentacene triplet excitons with chemical sensitivity. *Communications Physics* **2019**, *2*, 56.

(32) Purvis, G. D.; Bartlett, R. J. A Full Coupled-cluster Singles and Doubles Model: The Inclusion of Disconnected Triples. *The Journal of Chemical Physics* **1982**, *76*, 1910–1918.

(33) Scuseria, G. E.; Scheiner, A. C.; Lee, T. J.; Rice, J. E.; Schaefer, H. F. The Closed-Shell Coupled Cluster Single and Double Excitation (CCSD) Model for the Description of Electron Correlation. A Comparison with Configuration Interaction (CISD) Results. *J. Chem. Phys.* **1987**, *85*, 2881.

(34) Lee, T. J.; Rice, J. E. An Efficient Closed-Shell Singles and Doubles Coupled-Cluster Method. *Chemical Physics Letters* **1988**, *150*, 406–415.

(35) Sekino, H.; Bartlett, R. J. A Linear Response, Coupled-Cluster Theory for Excitation Energy. *Int. J. Quantum Chem.* **1984**, *26*, 255–265.

(36) Geertsen, J.; Rittby, M.; Bartlett, R. J. The Equation-of-Motion Coupled-Cluster

Method: Excitation Energies of Be and CO. *Chemical Physics Letters* **1989**, *164*, 57–62.

(37) Stanton, J. F.; Bartlett, R. J. The equation of motion coupled-cluster method. A systematic biorthogonal approach to molecular excitation energies, transition probabilities, and excited state properties. *The Journal of chemical physics* **1993**, *98*, 7029–7039.

(38) Koga, N.; Morokuma, K. Determination of the lowest energy point on the crossing seam between two potential surfaces using the energy gradient. *Chemical Physics Letters* **1985**, *119*, 371–374.

(39) Coriani, S.; Koch, H. Communication: X-ray absorption spectra and core-ionization potentials within a core-valence separated coupled cluster framework. *The Journal of Chemical Physics* **2015**, *143*, 181103.

(40) Carbone, J. P.; Cheng, L.; Myhre, R. H.; Matthews, D.; Koch, H.; Coriani, S. In *State of The Art of Molecular Electronic Structure Computations: Correlation Methods, Basis Sets and More*; Ancarani, L. U., Hoggan, P. E., Eds.; Advances in Quantum Chemistry; Academic Press, 2019; Vol. 79; pp 241–261.

(41) Sarangi, R.; Vidal, M. L.; Coriani, S.; Krylov, A. I. On the basis set selection for calculations of core-level states: different strategies to balance cost and accuracy. *Molecular Physics* **2020**, *118*, e1769872.

(42) Krishnan, R.; Binkley, J. S.; Seeger, R.; Pople, J. A. Self-consistent molecular orbital methods. XX. A basis set for correlated wave functions. *The Journal of chemical physics* **1980**, *72*, 650–654.

(43) Clark, T.; Chandrasekhar, J.; Spitznagel, G. W.; Schleyer, P. V. R. Efficient diffuse function-augmented basis sets for anion calculations. III. The 3-21+ G basis set for first-row elements, Li–F. *Journal of Computational Chemistry* **1983**, *4*, 294–301.

(44) Matthews, D. A.; Cheng, L.; Harding, M. E.; Lipparini, F.; Stopkowicz, S.; Jagau, T.-C.; Szalay, P. G.; Gauss, J.; Stanton, J. F. Coupled-cluster techniques for computational chemistry: The CFOUR program package. *The Journal of Chemical Physics* **2020**, *152*, 214108.

(45) Zhao, Y.; Truhlar, D. G. The M06 suite of density functionals for main group thermochemistry, thermochemical kinetics, noncovalent interactions, excited states, and transition elements: two new functionals and systematic testing of four M06-class functionals and 12 other function. *Theoretical Chemistry Accounts* **2008**, *120*, 215–241.

(46) Becke, A. D. A new mixing of Hartree–Fock and local density-functional theories. *The Journal of chemical physics* **1993**, *98*, 1372–1377.

(47) Tamm, I. In *Selected Papers*; Bolotovskii, B. M., Frenkel, V. Y., Peierls, R., Eds.; Springer Berlin Heidelberg: Berlin, Heidelberg, 1991; pp 157–174.

(48) Dancoff, S. M. Non-Adiabatic Meson Theory of Nuclear Forces. *Phys. Rev.* **1950**, *78*, 382–385.

(49) Salazar, E.; Faraji, S. Theoretical study of cyclohexadiene/hexatriene photochemical interconversion using spin-Flip time-Dependent density functional theory. *Molecular Physics* **2020**, *118*, e1764120.

(50) Shao, Y. et al. Advances in molecular quantum chemistry contained in the Q-Chem 4 program package. *Molecular Physics* **2015**, *113*, 184–215.

(51) Kajimoto, O.; Yokoyama, H.; Ooshima, Y.; Endo, Y. The structure of 4-(N, N-dimethylamino) benzonitrile and its van der Waals complexes. *Chemical physics letters* **1991**, *179*, 455–459.

(52) Heine, A.; Herbst-Irmer, R.; Stalke, D.; Kühnle, W.; Zachariasse, K. A. Structure and crystal packing of 4-aminobenzonitriles and 4-amino-3, 5-dimethylbenzonitriles at

various temperatures. *Acta Crystallographica Section B: Structural Science* **1994**, *50*, 363–373.

(53) Parusel, A. B.; Köhler, G.; Grimme, S. Density functional study of excited charge transfer state formation in 4-(N, N-dimethylamino) benzonitrile. *The Journal of Physical Chemistry A* **1998**, *102*, 6297–6306.

(54) Matthews, D. A. EOM-CC Methods with Approximate Triple Excitations Applied to Core Excitation and Ionisation Energies. *Molecular Physics* **2020**, *118*, e1771448.

(55) Gómez, I.; Reguero, M.; Boggio-Pasqua, M.; Robb, M. A. Intramolecular Charge Transfer in 4-Aminobenzonitriles Does Not Necessarily Need the Twist. *Journal of the American Chemical Society* **2005**, *127*, 7119–7129, PMID: 15884954.

TOC Graphic